

Giant Pulses from the Millisecond Pulsar B1821–24

Roger W. Romani^{1,2} and Simon Johnston³

ABSTRACT

We have carried out a survey for ‘giant pulses’ in 5 millisecond pulsars. We detect individual pulses from the high \dot{E} pulsar PSR B1821–24 with energies exceeding $50\times$ the mean pulse energy. These giant pulses are concentrated in a narrow phase window coincident with the power-law non-thermal pulse seen in hard X-rays. This is the third example of the giant pulse phenomenon. It supports the idea that large B fields in the outer magnetosphere are critical to the formation of such pulses and further suggests a direct connection between giant pulses and high energy emission.

Subject headings: pulsars: individual (PSR B1821–24)

1. Introduction

Despite three decades of intensive study, the mechanism producing pulsar radio emission is poorly understood. Fluctuations in the intensity of the radio radiation provide important constraints on plausible mechanisms. Single-pulse studies of bright pulsars detect a variety of patterns in the intrinsic intensity fluctuations, including nulling and drifting phenomena. The distribution of integrated pulse energies, however, has only a modest dispersion, typically forming a Gaussian of width $\lesssim \langle E \rangle$, the mean pulse energy (eg. Manchester & Taylor 1974). In contrast, the Crab pulsar PSR B0531+24 emits pulses with energies $> 20 \times \langle E \rangle$, extending up to $> 2 \times 10^3 \langle E \rangle$ (Lundgren et al. 1995) which were instrumental in the original detection of the Crab (Staelin & Reifenstein 1968). These Giant Pulses (GP) are typically broadband (Moffett 1997, Sallmen et al. 1999) and of short duration, with widths of order a few μs and structure down to 10ns (Hankins 2000). They are localized to the main and interpulse phase windows and follow an intensity distribution best characterized as a power law with

index of $\approx 3 - 3.5$.

The discovery of similar pulses from the millisecond pulsar PSR B1937+214 (Sallmen & Backer 1995, Cognard et al. 1996) was surprising. The pulses are extremely short ($\tau < 0.3\mu s$) events confined to small phase windows trailing the main and inter-pulses, again with an approximately power-law distribution of pulse energies (Kinkhabwala & Thorsett 2000). Since PSR B1937+214 is the only known radio pulsar having an estimated magnetic field at the light cylinder larger than that of the Crab, it has been suggested that this is a key parameter controlling the giant pulse phenomenon (Cognard et al. 1996).

Johnston et al. (2001) have recently found that the Vela pulsar produces pulses with a very wide distribution of peak fluxes. It is not clear if these events are related to true giant pulses; the largest such pulses observed to date have $E < 10\langle E \rangle$, but these narrow pulses have peak fluxes exceeding $40\times$ the integrated peak intensity. Relatively few individual pulses have been examined, and the extended tail in the E distribution of these ‘giant μ -pulses’ may continue into the true GP regime. The pulses are localized to a phase window off of the integrated pulse emission, are of short duration and are highly polarized.

To explore the connection between the Crab and PSR B1937+214 GPs and the large individual pulses of $1 - 3 \times 10^4$ yr Vela-like pulsars, we

¹Dept. of Physics, Stanford University, Stanford CA 94305-4060

²Visiting Scholar School of Physics, University of Sydney & ATNF, CSIRO, Epping, NSW

³School of Physics, University of Sydney, NSW 2006, Australia

obtained fast time sample data for several young and millisecond pulsars. We report here evidence for giant pulses in the MSP with the next highest known light cylinder field, PSR B1821–24, along with limits on GP emission in other high-field MSPs. In a companion paper (S. Johnston & R.W. Romani 2001, in preparation) we discuss large individual pulse energies in young high field pulsars.

2. Observations

Observations were made on 20-22 May 2001, with the Parkes 64-m radio telescope. We used the center beam of the 21-cm multi-beam system at an observing frequency of 1517.75 MHz. The receiver has a system equivalent flux density of 30 Jy on cold sky. The back-end consisted of a filterbank containing 512 channels per polarization each of width 0.5 MHz for a total bandwidth of 256 MHz. The polarization pairs are summed, each output is then sampled at 80 μ s, one-bit digitized, and written to DLT for off-line analysis.

The data were then de-dispersed at the pulsar’s nominal dispersion measure. The mean and rms of groups of 8192 samples (0.65 s) were examined and those which showed obvious signs of interference were discarded. The data could then be folded synchronously with the pulsar’s topocentric period to produce a pulse profile. Our nominal 5- σ sensitivity in 80 μ s is 1.3 Jy. In practice, even after clipping, we experienced substantially larger background fluctuations and the rms exceeded our expected rms by a factor of 1.5-3.

To confirm that we could detect conventional GPs we made short observations of the Crab pulsar, during which GPs were detected with high significance. Short integrations with the Vela pulsar off-axis, producing an effective continuum flux of only 0.6 mJy, confirmed that we could detect the largest individual Vela-type giant μ -pulses at these faint continuum flux levels. Finally, and most relevant to the present study we observed PSR B1937+214, obtaining 1784s of integration (1.15×10^6 pulses). Our sampling provides only 19 bins across the pulse profile, but we clearly detect the GP distributions in both the main and interpulse components. In both components the giant pulse peaks occur approximately one bin after the corresponding peak of the integrated pulse

profile. The largest main component GP obtained had an energy 445 Jy μ s, the third largest had 230 Jy μ s. The phasing and intensity distribution are well matched to the 1.4 GHz results reported by Kinkhabwala & Thorsett (2000).

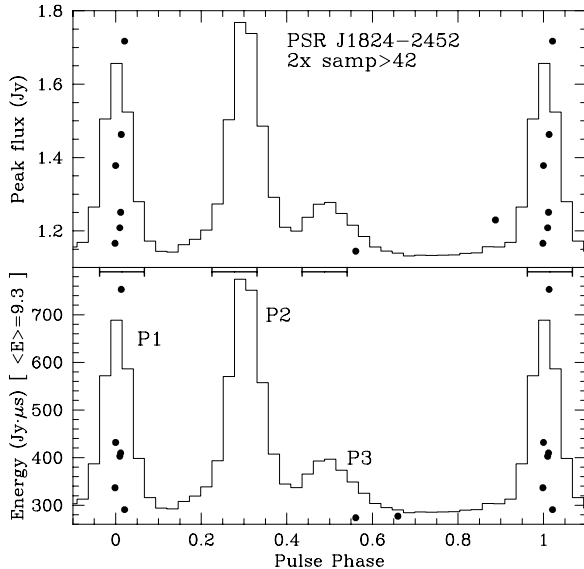


Fig. 1.— Giant pulses from PSR B1821–24. Upper panel: the peak flux of the brightest pulses with adjacent bins $> 4\sigma$, points at the peak phase. Our integrated profile (arbitrary scale) is overplotted for reference; 1.2 periods are shown. Lower panel: Integrated energy of the brightest GP. We label the components on the reference pulse profile and mark (at top) the 4-bin windows used to measure component energies.

3. Results

PSR B1821–24 has a period of 3.05 ms and a dispersion measure (DM) of 119.8 cm^{-3}pc . This DM leads to a smearing of 142 μ s across our 0.5 MHz filter bands, limiting our resolution and ensuring that any giant pulse from the source will be smeared across 2-3 time samples. We obtained 3×3600 s of data on this pulsar starting at MJD 52049.7; after excision of 0.65 s averages showing strong interference, we retained 9943 s of data or $\approx 3.3 \times 10^6$ pulses. Because of the expected DM smearing, we first searched the de-dispersed data stream by tagging pulses with 2 or more consecutive samples exceeding 4σ . Our data contained

16 such pulses. The brightest of these, both in terms of peak sample intensity and integrated energy were confined to a narrow window in the first component of the integrated pulse profile (Figure 1, which shows the brightest 8 pulses by each measure). During these observations PSR B1821–24 had a continuum flux of ≈ 3 mJy and an average pulse energy of $9.3 \text{ Jy } \mu\text{s}$. The largest individual pulse observed had $E \approx 755 \text{ Jy } \mu\text{s}$ which is $81 \langle E \rangle$.

This pulsar has a complex pulse morphology. We adopt the naming convention of Backer & Sallmen (1997), in which P1 has a steep spectrum, dominating the pulse at low radio frequencies and the second narrow pulse P2 is stronger at short wavelength. The broad trailing component P3 seems to have a similar spectrum to P1. Backer & Sallmen report that at 1.4 GHz the pulsar occasionally spends many hours in a mode with P2 decreased relative to the other components by a factor of 4. We do not see such dramatic variations, but confirm that P2 is variable, decreasing in flux by 25% relative to P1 and P3 over our first hour of integration and stabilizing afterwards.

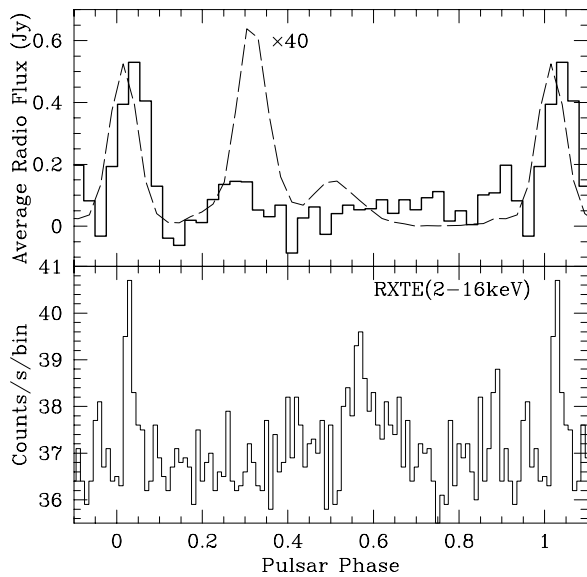


Fig. 2.— Above: the average profile of the 16 GP candidates (full line histogram) compared with the average profile of all pulses, magnified by $40\times$ (dashed line curve). Below: the *RXTE* pulse profile with the relative phase determined by Rots et al. (1998).

The pulsar is also detected in the X-ray, again

with a complex pulse profile. Careful timing (Rots et al. 1998) using the *Rossi X-ray Timing Explorer (RXTE)* establishes that the narrow, hard spectrum X-ray component is associated with P1, but lags significantly by $60 \pm 20 \mu\text{s}$. A second broad, and apparently softer, X-ray peak lags P3 by $250 \pm 60 \mu\text{s}$. Figure 2 compares our integrated pulse profile and the profile obtained by averaging all 16 pulses with adjacent samples $> 4\sigma$. These pulses have been re-sampled to common phase bins, with 38 points across the light curve; each bin corresponds to about one original sample. The ‘GP’ lightcurve P1 emission lags that of the integrated pulse profile by approximately $80 \mu\text{s}$ (one bin). No other significant GP feature is seen. For comparison we plot the *RXTE* light curve of Rots et al. , with the relative phasing determined in that study. DM smearing and re-sampling to fixed phase windows can fully account for our GP pulse width. Thus our GP emission appears to be unresolved in phase and coincident with the hard power law high energy pulse.

We can obtain some further information on the GP distribution by measuring pulse intensity distributions in windows of pulse phase. For each pulse we defined a 10 sample off pulse window ($\phi = 0.63-0.85$ in Figure 1). The individual components were estimated by the three 4-sample windows indicated in Figure 1 (P1= $-0.03 - 0.05$; P2= $0.24 - 0.32$; P3= $0.45 - 0.53$). For each pulse we determined the background level from the median of the samples in off pulse region of the current and preceding pulses. The individual component energy was measured by an integration of the energy in the appropriate four sample window. The cumulative histograms of the three components are shown in Figure 3. Component P1 shows an appreciable excess of high energy pulses, extending somewhat below our selected giant pulse threshold. Note that due to DM smearing and our limited resolution, some pulse energy will be lost from these 4-sample windows, so these E values underestimate the full pulse energy.

Since only our brightest GPs are well separated from the underlying pulse and noise fluctuations, we can put little constraint on their intensity distribution. Power law indices of $\approx 3 - 5$ adequately describe the GP excess. Indeed an addition of an E^{-5} power law to the P3 flux distribution nominally matches the P1 distribution quite

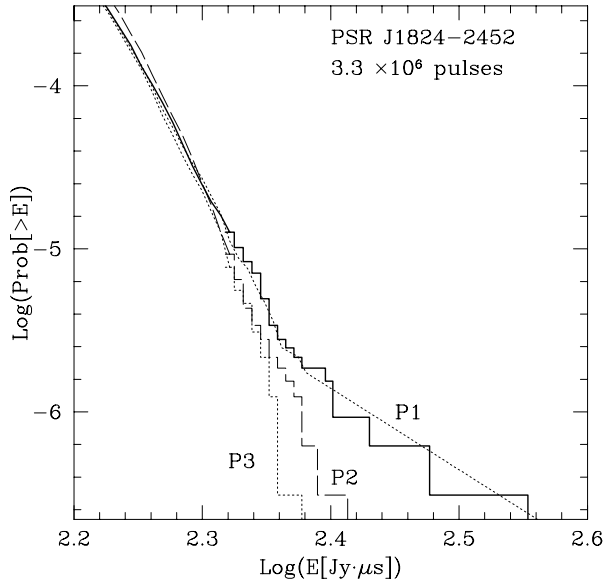


Fig. 3.— Cumulative probability distributions of pulse energy in our three selected pulse component windows. The probability histograms are continued as smooth lines at low pulse energies. There P2 is the highest, as expected from the average pulse profile. At large energies there is a clear excess in component P1 (full line histogram). A simple power law for the excess GP distribution is plotted with the dashed line.

well (dashed smooth line). As for the 1.4 GHz PSR B1937+214 data of Kinkhabwala & Thorsett (2000), it is likely that noise fluctuations and normal pulses steepen the estimated power law index this close to the noise floor. Longer observations with greater sensitivity will be needed to probe the true GP intensity distribution. We expect about 1/h ($P \approx 8.5 \times 10^{-7}$) with $E > 28\langle E \rangle$. This 1.4 GHz GP rate is, in fact, roughly twice that of PSR B1937+214, which has $P(28\langle E \rangle) \approx 4 \times 10^{-7}$.

If our GP are as narrow as those of PSR 1937+214, we expect the brightest pulse in an hour to reach a peak flux of $\gtrsim 1300$ Jy.

4. Limits for other MSPs

We also observed four other millisecond pulsars with high inferred light cylinder magnetic fields, B_{LC} . In Table 1, in B_{LC} order, the pulsars that we observed are listed along with the mean pulse energy, number of pulses observed and the limit to which giant pulses were not seen. These four pulsars have B_{LC} s substantially lower than that of PSR B1821–24. For PSRs J0034–0534, J2129–5721 and J1911–1114, the low flux at our observation epoch precluded significant bounds on GP emission. The last entry of the table lists the factor by which a pulse must exceed $\langle E \rangle$ to be detected in our study. Indeed, if the cumulative intensity distribution followed $\text{Prob}(> E) \propto E^{-3}$ and the GP rate were the same as for B1821–24, we would have required 10^5 , 58 and 18 million pulses, respectively, to see a giant pulse in these three pulsars at our achieved threshold. Considering further the likely decreased GP frequency at lower B_{LC} , our limits do not significantly constrain GP emission in these sources. On the other hand, for J0613–0200 (with a similar period and flux density to PSR B1821–24 but B_{LC} lower by 5), our limits do begin to probe B1821–24-like GPs. For the GP distribution assumed above with the same probability as in B1821–24, we would have expected about 15 GP events. In fact, the largest few pulses do occur in 0.1 of phase ahead of the integrated pulse profile, suggesting that more sensitive observations might uncover a GP distribution in this source at $\lesssim 1/10$ the frequency of the events seen in B1821–24.

Table 1. MSP Giant Pulse Candidates

Name	P (ms)	B_{LC} ($\times 10^5$ G)	DM (cm^{-3} pc)	$\langle E \rangle$ (Jy μ s)	N_p ($\times 10^6$)	E_{lim} ($\langle E \rangle$)
B1821–2452	3.1	7.2	120	9.3	3.3	[†] 20-80
J0034–0534	1.9	1.4	14	0.1	1.9	2000
J0613–0200	3.1	0.55	39	9.2	4.6	27
J2129–5721	3.7	0.50	32	1.9	2.9	155
J1911–1114	3.6	0.44	31	2.6	1.5	105

[†] GP detections

5. The Giant Pulse Phenomenon and High-Energy Emission

The addition of B1821–24 to the GP family supports the idea that large magnetic fields in the outer magnetosphere are required for this behavior. However this object points to an additional common feature: as for the Crab pulsar, the GPs appear isolated to narrow windows of pulse phase showing high energy pulses, with hard power law spectra. In the case of the Crab these X- and γ -ray pulses are believed to arise in an outer magnetosphere acceleration gap along the boundary of the open zone (Cheng, Ho & Ruderman 1986; Romani & Yadigaroglu 1995). These Crab-type outer gaps are believed to have $\gamma - \gamma$ pair production maintained by a dense bath of target soft synchrotron photons from the gap itself. High B fields (especially near the null charge surface) should enhance this synchrotron emissivity, and hence the rate of secondary e^\pm production. This dense pair plasma produces the narrow hard X-ray pulses, and we can speculate that the high densities promote the instabilities that create enhancements in the particle coherence and hence the giant radio pulses.

This picture provides a few predictions. PSR B1937+214 shows narrow X-ray pulses in ASCA data (Takahashi et al. 2001), with a phase close to the radio interpulse. We expect that a high resolution X-ray profile with good absolute radio phase comparison will show these X-ray pulses to align with the GP phase, lagging the integrated radio profile pulse peak. It is not clear why the interpulse should be stronger at high energies than the main pulse. An additional strong GP candidate not accessible to our survey is the millisecond pulsar PSR J0218+4232 ($B_{LC} = 3.1 \times 10^5$ G). Comparison with the high energy pulse profile (Kuiper et al. 2000) suggests that GP emission may be found in the second radio pulse, and possibly in the > 100 MeV pulse phase preceding the first radio peak.

The detailed dependence of the GP frequency on B_{LC} is not clear. If the critical quantity is the field near the outer gap base at the null charge surface, where pair production is expected to be most intense, then magnetic inclination α can have a strong effect with $B \approx B_{LC}[1.5 \tan(\alpha)]^6$ for a static dipole field and $\alpha \gtrsim 30^\circ$. Consider the case of the Crab pulsar, which has a frequency

of $E > 20\langle E \rangle$ pulses roughly $10^4 \times$ larger than that of PSR B1937+214 or PSR B1821–24 at 1.4 GHz. Polarization modeling (Romani and Yadigaroglu 1995) and the recent CXO wind torus images suggest that the Crab has $\alpha \approx 80^\circ$. Baker and Sallmen (1997) found a plausible polarization sweep fit of $\alpha \approx 50^\circ$ for PSR B1821–24. For this angle the nominal field at the base of the gap is suggestively $10^4 \times$ lower than that of the Crab. Of course, the magnetosphere of a MSP is likely far from vacuum dipole, but this does underline that α can have a strong effect on the ordering of GP candidates by B .

A better criterion for the presence of strong GP activity may be the presence of a narrow hard spectrum X-ray pulse, indicating a dense pair plasma in an active outer gap. Most known, young γ -ray pulsars are Vela-like with pair production controlled by thermal surface fluxes (e.g. Romani 1996). These do have non-thermal X-ray pulse components, but these are much broader and the emission represents a much smaller fraction of the spindown luminosity. GP distributions might therefore be much weaker in these pulsars. The occurrence of GP in other young Crab-like pulsars and the connection with the large pulses from millisecond pulsars described here can only be addressed by further sensitive single pulse studies.

The Parkes telescope is funded by the Commonwealth of Australia for operation as a National Facility managed by CSIRO. The 512 channel filterbank system used in the observations was designed and built at the Jodrell Bank Observatory, University of Manchester. Observing software was provided by the Pulsar Multibeam Survey group.

REFERENCES

- Backer, D.C. & Sallmen, S. T. 1997, *AJ*, **114**, 1539
 Cognard, I., Shrauner, J.A., Taylor, J.H. & Thorsett, S.E. 1996, *ApJ*, **457**, L81
 Cheng, K.S., Ho, C. & Ruderman, M.A. 1986, *ApJ*, **300**, 522.
 Hankins, T. 2000, *ASP Conf Ser.*, **202**, 165.
 Johnston, S., van Straten, W., Kramer, M. & Bailes, M. 2001. *ApJ*, **549**, L101.
 Johnston, S. & Romani, R.W. 2001, in prep.

- Kinkhabwala, A. & Thorsett, S.E. 2000, *ApJ* **535**, 365
- Kuiper, L. et al. 2000 *AA*, **359**, 615.
- Lundgren, S.C. et al. 1995 *ApJ*, **453**, 433.
- Manchester, R.N. & Taylor, J.H. 1977, *Pulsars*, (Freeman:San Francisco).
- Moffett, D.A. 1997, PhD Thesis, New Mexico Inst. Mining and Technology
- Romani, R.W. 1996, *ApJ*, **470**, 469.
- Romani, R.W. & Yadigaroglu, I.-A. 1995, *ApJ*, **438**, 314
- Rots, A.H. et al. 1998, *ApJ*, **501**, 749
- Sallmen, S., et al. 1999, *ApJ*, **517**, 460
- Sallmen, S. & Backer 1995, *ASP Conf. Ser.*, **72**, 340.
- Takahashi, M. et al. 2001, *ApJ*, **554**, 316.